



DØnote 4859-CONF

The Isolated Photon Cross Section in the Central Rapidity Region at 1.96 TeV.

The DØ Collaboration

URL: <http://www-d0.fnal.gov>

(Dated: June 24, 2005)

A measurement of the inclusive cross section for production of isolated photons is presented for transverse energies in the range of 23–300 GeV in the central pseudorapidity region $|\eta| < 0.9$. The results are based on a data sample of 325.9 pb^{-1} of integrated luminosity accumulated during 2002–2004 in $p\bar{p}$ collisions at $\sqrt{s} = 1.96 \text{ TeV}$ and recorded with the DØ detector at the Fermilab Tevatron Collider. The results are compared with the next-to-leading order QCD predictions.

Preliminary Results for Summer 2005 Conferences

I. INTRODUCTION

Production of isolated photons in high energy hadronic collisions has been studied extensively both theoretically and at experiments during the last 20 years. In high energy $p\bar{p}$ collisions the dominant source for production of photons with moderate and high transverse momentum p_T is direct (or prompt) photons. They are called direct since they are produced directly from parton-parton interactions and not from the hadron decays (such as π^0, η, K_s^0). These photons come unaltered from the hard process and therefore can give us a clean test of the hard scattering dynamics. Direct-photon production is complimentary to deep inelastic scattering, Drell-Yan pair production and to inclusive production of jets. Photon identification is free from the uncertainties caused by the fragmentation of partons into hadrons or by experimental issues related to jet identification and energy measurement and thus has an advantage over jet production measurement.

In the region up to $p_T^\gamma \simeq 150$ GeV direct photons are mainly produced through the Compton scattering $qg \rightarrow q\gamma$ [1] and thus their production cross section is sensitive to the gluon density inside the colliding hadrons. A high center of mass energy at the Tevatron and the statistics accumulated currently in Run II allows us to test quantum chromodynamics (QCD) and gluon distribution in the region of large Q^2 and in a wide range of x_T : $0.02 < x_T < 0.30$. Measurements of the isolated photon cross section also allows tests of the next-to-leading order (NLO) and resummed QCD calculations, phenomenological models of gluon radiation, studies of photon isolation and the fragmentation process. In addition, photons in the final state may be an important sign of new particles and/or physics beyond the standard model. Thus, first of all, it is useful and necessary to study and to understand the “conventional” sources of photons.

This note presents a first measurement of the cross section for production of isolated photons in $p\bar{p}$ collisions at $\sqrt{s} = 1.96$ TeV (Run II) in the central pseudorapidity region of $|\eta| < 0.9$ [2], and covers a much wider p_T^γ range than Run I measurements at CDF [3] and DØ [4]. (Pseudorapidity is defined as $\eta = -\ln \tan\theta/2$, where θ is the polar angle with respect to the proton beam.)

II. ANALYSIS

A. Selection Criteria.

Photon candidates were identified in the DØ detector [5] as isolated clusters of energy depositions in the uranium and liquid-argon sampling calorimeter. The electromagnetic (EM) section of the calorimeter is segmented longitudinally into four layers (EM1-EM4) of 2, 2, 7, and 10 radiation lengths respectively, and transversely into cells in pseudorapidity and azimuthal angle $\Delta\eta \times \Delta\phi = 0.1 \times 0.1$ (0.05×0.05 in EM3). In addition, the cluster may also contain the energy deposited in the hadronic portion of the calorimeter located behind the EM one [5].

To select photon candidates in data and Monte Carlo (MC) we have used the following criteria. Each EM cluster-photon candidate is formed by a simple cone algorithm with the cone size of $\mathcal{R} = \sqrt{\Delta\eta^2 + \Delta\phi^2} = 0.2$ [4]. The data were initially preselected with the requirement of at least one EM cluster with $p_T > 15$ GeV. The preselected events are required to pass a combination of the unprescaled EM triggers [4]. The event vertex was required to be within 50 cm of the nominal center of the detector along the beam ($|Z_{vtx}| < 50$ cm) and should have at least 3 associated tracks.

Candidate EM clusters were accepted within the pseudorapidity region $|\eta| < 0.9$. To avoid inter-calorimeter boundaries and cracks, EM fiducial cuts were applied. The total geometric acceptance was found to be 0.842 ± 0.002 . Each candidate was required to deposit more than 95% of the detected energy in the EM section of the calorimeter ($\text{EMfrac} > 0.95$) and to be isolated in the annular region between $\mathcal{R} = 0.2$ and $\mathcal{R} = 0.4$ around the energy-weighted centroid: $\text{Iso}(\Delta\mathcal{R}02) < 0.10$. Here $\text{Iso}(\Delta\mathcal{R}02) = (\text{EisoTot} - \text{EisoCore})/\text{EisoCore}$, where EisoTot is the overall (EM+hadronic) tower energy in the (η, ϕ) cone of $\mathcal{R} = 0.4$ and EisoCore is the EM tower energy in the cone of $\mathcal{R} = 0.2$. The probability to have any track spatially matched to the EM cluster in the event was required to be below 0.001. We also reject events having too large missing E_T by the cut $E_T^{\text{miss}}/p_T^\gamma < 0.7$. The photon selection efficiency with respect to these cuts is presented in Fig. 1. It can be fitted by $a - \exp[(b - p_T)/c]$ with $a = 0.915 \pm 0.004$, $b = -52.04 \pm 6.11$, and $c = 28.43 \pm 1.60$.

A set of additional four variables was used for further background suppression. They are the number of the EM cluster cells at the EM1 layer with a cell energy $E_{\text{cell}} > 0.4$ GeV, the number of cells around the EM cluster within the ring of $0.2 < \mathcal{R} < 0.4$ with the same E_{cell} threshold, the scalar sum of track transverse momenta in the ring of $0.05 < \mathcal{R} < 0.4$ with $p_T^{\text{track}} > 0.3$ GeV, and the energy-weighted EM cluster width in $r \times \phi$ at the EM3 layer. These variables showed consistent behavior from the point of view of the MC/data comparison of the electrons and positrons from $Z \rightarrow e^+e^-$ events.

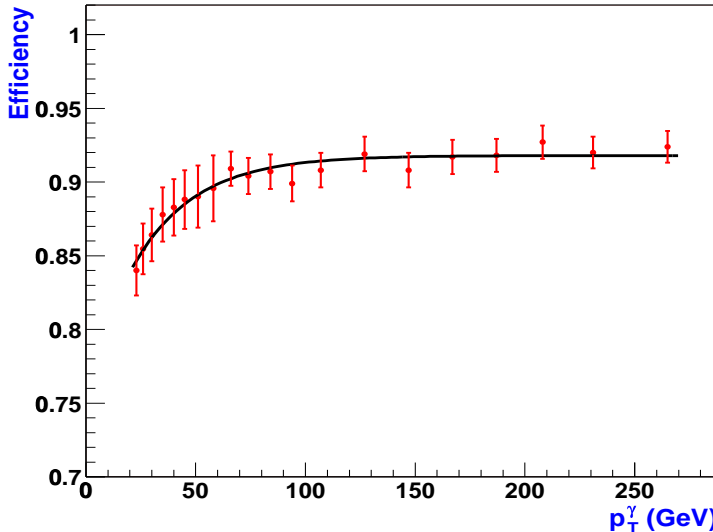


FIG. 1: Photon selection efficiency to pass the main cuts: Events satisfy conditions $\text{EMfrac} > 0.95$, $\text{Iso}(\Delta\mathcal{R}02) < 0.10$, no spatially matched tracks and $E_T^{\text{miss}}/p_T^\gamma < 0.70$ as a function of p_T . The efficiency is fitted by function $a - \exp[(b - p_T)/c]$ with $a = 0.915 \pm 0.004$, $b = -52.04 \pm 6.11$, and $c = 28.43 \pm 1.60$.

When discriminating between direct photons and photons from backgrounds such as π^0 decays, we face a problem of pattern recognition. Most discriminant variables cannot separate the two event classes unambiguously. The standard procedure for solving such a problem is the introduction of relevant cuts in the multi-dimensional data. Nowadays the application of a software-implemented artificial neural network (ANN) for pattern recognition is well established and usually gives results that are superior to conventional approaches [6]. So, instead of direct application of cuts on these variables they were used to build an ANN that can accumulate a power of all four variables and separate criteria on them. The ANN, based on the JETNET package [7], is then applied for an additional selection criterion and subsequent calculation of photon purity. The ANN is trained to discriminate between MC direct photons from “ γ^{dir} + jet” events (taken as the signal) and EM jets (taken as the background). The latter are QCD jets, generated with the MC event generator PYTHIA [8], that have passed the main selection criteria: $\text{EMfrac} > 0.95$, $\text{Iso}(\Delta\mathcal{R}02) < 0.10$ and have no spatially matched track. The network is trained to produce unity in case of a signal and zero in case of a background event.

We select the events that have a network output value greater than 0.5. A systematic error assigned to this cut is the difference between the efficiencies for MC and data electrons/positrons from $Z \rightarrow e^+e^-$ events and is 2.4%. The photon efficiency with respect to this cut is 0.937 ± 0.002 and is independent of p_T^γ . The distributions over the ANN output for the MC direct photon, em-jets and data for $44 < p_T^\gamma < 50$ GeV are presented in Fig. 2 with the position of the cut.

B. Photon Purity Estimation.

The signal from direct photons is contaminated with backgrounds from jets that have fluctuated into well-isolated EM clusters. These jets are primarily composed of one or more neutral mesons that decay into photons, and may also be accompanied by other soft hadrons whose energies are deposited in the EM portion of the calorimeter.

Since the signal events cannot be identified on an event-by-event basis, their photon fraction (purity) \mathcal{P} is determined for a given p_T^γ bin statistically. The photon purity is defined as a ratio

$$\mathcal{P} = \frac{N^\gamma}{N^\gamma + N^{\text{jet}}} \quad (1)$$

where N^γ (N^{jet}) is the number of single photons (QCD jets) that passed the selection criteria.

The ANN output in data is fitted to ANN outputs from MC photon and em-jet samples by using the HMCMLL routine [9]. This fitting procedure correctly incorporates the statistical error from both the MC and data inputs. The uncertainty of the measured purity points is mostly caused by the statistics of the QCD jet sample which remains after passing the main selection cuts while for high p_T intervals it is mostly caused by data statistics.

The photon fractions determined from HMCMLL were fitted by function (2)

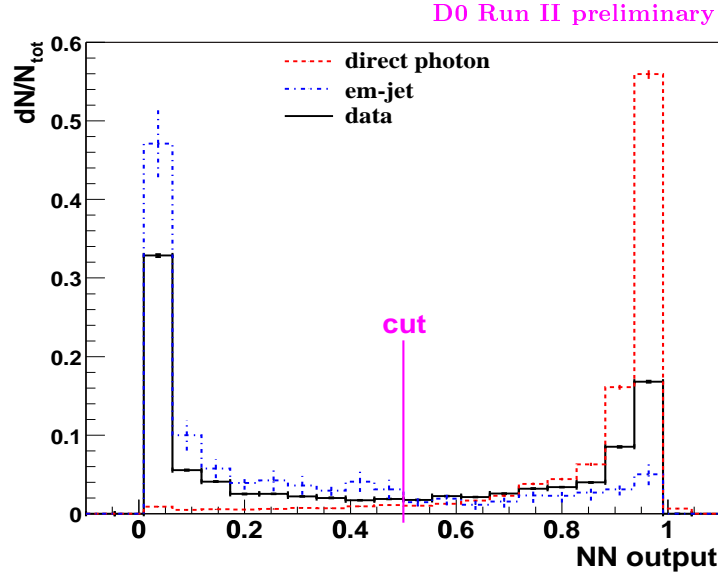


FIG. 2: Normalized distribution of the ANN output for data, signal and background events from interval of $44 < p_T^\gamma < 50$ GeV after application of the main selection criteria: $\text{EMfrac} \geq 0.95$, $I\text{so}(\Delta R02) \leq 0.10$, no spatially matched tracks and $E_T^{\text{miss}}/p_T^\gamma < 0.70$. The cut position is shown.

$$\mathcal{P}_f = 1/(1 + a (p_T^\gamma)^b) \quad (2)$$

We have chosen this form because we expect the data to be a sum of two falling cross sections (photons and jets) with their ratio having roughly the form $a(p_T)^\beta$ (compare with formula (1)). Values of the two free parameters found from fit are $a = 38.86 \pm 16.71$ and $\beta = -0.971 \pm 0.112$. Apart from the main fitting function two other functions can be used: $\mathcal{P}_f = 1 - \exp(a + b p_T^\gamma)$ and $\mathcal{P}_f = a + b \ln(p_T^\gamma)$. In Fig.3 we plot the default fit with its statistical error as well as the systematic band in uncertainty caused by usage of alternative fitting functions and by variation of the number of bins in the HMCMLL fit. The fit, shown in Fig. 3 with its statistical uncertainty, assures that purity is a smooth function of p_T^γ .

An additional systematic uncertainty was assigned due to the fragmentation model used in the generator PYTHIA [8]. This uncertainty was estimated by varying the ratio between π^0 and η, K_s^0, ω (containing γ/π^0 in the decay channel) by $\pm 50\%$. Such a variation mostly influences the region up to ~ 50 GeV and leads to an additional systematical error

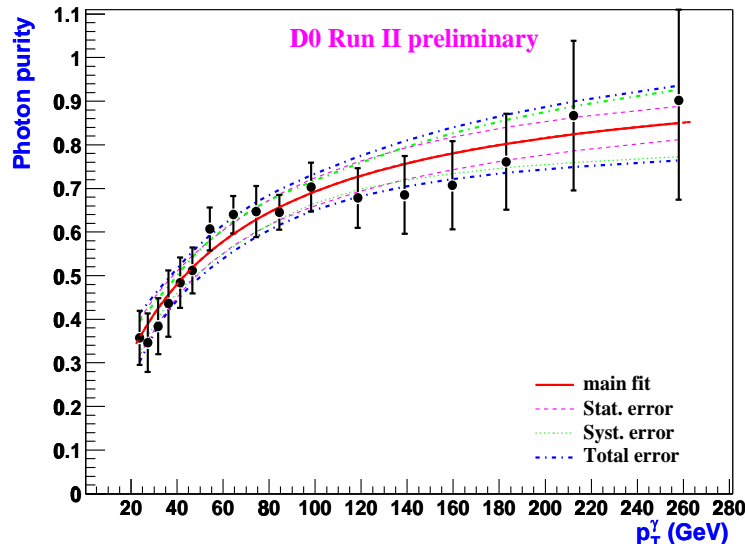


FIG. 3: Dependence of the photon purity on p_T^γ . The figure shows default fit (red full line), statistical error from the default fit (purple dashed line), band in systematic uncertainty (green dotted line) and total error (blue dash-dotted line).

of about 7% in purity at $p_T^\gamma \simeq 25$ GeV, 2% at $p_T^\gamma \simeq 50$ GeV and 1% at $p_T^\gamma \gtrsim 70$ GeV.

C. Photon Energy Scale and Unsmearing Corrections.

The calorimeter layer weights used to reconstruct the initial energy of the electromagnetic particle were found by using electron based ($Z \rightarrow ee$, $J/\psi \rightarrow ee$) events. Because of differences in the development of electromagnetic showers, photons lose noticeably less energy in the material in front of the calorimeter than electrons. This fact can lead to a systematic over-correction in the energy of photons and would yield a shift in the cross section. The Monte Carlo simulated “photon+jet” events were used to find the necessary corrections. They turned out to be around 1.9% at $p_T^\gamma \simeq 20$ GeV, 1.0% at 40 GeV and negligibly small at $p_T^\gamma \geq 70$ GeV.

Unsmearing is correcting a cross section due to the finite resolution of the calorimeter. It is especially important for the case of a steeply falling spectrum. The unsmearing of p_T^γ spectra was performed with an analytical method, fitting to the uncorrected cross section a function obtained by the convolution of an initial ansatz (as a physical distribution) and an energy resolution function. The correction factors f_{unsm} were then obtained as a ratio of the unsmeared (physical) to smeared fitted function. The correction can be parametrized by the linear function $f_{unsm} = a - b \cdot p_T^\gamma$ with $a = 0.971 \pm 0.002$ and $b = (0.906 \pm 0.143) \times 10^{-4}$.

III. CALCULATION OF CROSS SECTION AND COMPARISON WITH THEORY.

The inclusive photon cross section was obtained by the relation

$$\frac{d^2\sigma}{dp_T^\gamma d\eta^\gamma} = \frac{N \mathcal{P} f_{unsm}}{\mathcal{L}_{int} \Delta p_T^\gamma \Delta \eta^\gamma A \epsilon_t \epsilon_s} \quad (3)$$

where N is the number of photon candidates in the selected sample, \mathcal{P} is the photon purity, f_{unsm} is the unsmearing correction factor, \mathcal{L}_{int} is the integrated luminosity, Δp_T^γ and $\Delta \eta^\gamma$ are the bin sizes in transverse momentum and pseudorapidity, A is the geometric acceptance, ϵ_t is the trigger efficiency, and ϵ_s is the efficiency of the selection criteria.

The total number of photon candidates remaining after the analysis of the initial data set collected with $\mathcal{L}_{int} = 325.9 \pm 21.2$ pb $^{-1}$ and application of all the selection criteria is about 2.7 million. They were used to calculate the cross section in 17 p_T^γ bins with average values varying from 23.9 to 258.0 GeV.

The preliminary results of the measurement are shown in Fig. 4 as a function of p_T^γ for the central pseudorapidity region $|\eta^\gamma| < 0.9$ with the total experimental (systematic \oplus statistical) errors. The data are plotted at the p_T^γ -weighted average of the fit function for each bin.

One can see that in the presented range of $23 < p_T^\gamma < 300$ GeV the central photon cross section falls by about 5 orders of magnitude. Statistical errors vary from 0.1% in the first p_T^γ bin to 13.2% in the last bin, while systematic errors range from 11 to 25%. The largest source of systematic uncertainty is caused by the purity estimation (see Fig.3).

The superimposed theoretical curve corresponds to the QCD NLO predictions based on the JETPHOX program [10] (red full line) with the CTEQ6.1M set of parton distribution functions (PDF) [11]. The obtained results were also compared with the QCD NLO predictions [12] based on the small-cone approximation and using the same PDF. The two predictions are based on different sets of fragmentation functions, which are [13] in the first and [14] in the second case. Both predictions for the applied isolation and EM fraction limitations are found to be in agreement within 7%. Sensitivity of the theoretical predictions to the isolation requirements in the ring of $\Delta\mathcal{R} = 0.2$ and to the EM fraction in the cone of $\mathcal{R} = 0.2$ was tested [15]. Variation of the $Iso(\Delta\mathcal{R}02)$ cut from 10 to 5% and from 10 to 15% leads to changes in the predicted cross section of less than 2%. Variation of allowable hadronic energy in the cone of $\mathcal{R} = 0.2$ (i.e. inside of EM cluster) from 4 to 6% also leads to relative changes in the cross section $\leq 2\%$ [15].

The theoretical predictions presented in Fig. 4 correspond to the choice of renormalization, factorization and fragmentation scales as $\mu_R = \mu_F = \mu_f = p_T^\gamma$. If all scales are varied to $\mu_R = \mu_F = \mu_f = 0.5p_T^\gamma$ or to $2p_T^\gamma$, the cross sections change within $\pm 12\text{--}13\%$ (see Fig. 6).

The ratio of the theoretical predictions done with MRST2004 [16] to the ones with CTEQ6.1M is shown in Fig. 5. One can see that all variations are within 6 – 7%.

The ratio of the measured cross section to the NLO QCD predictions [10] calculated with the CTEQ6.1M PDF set is presented in Fig. 6. Ratios of the nominal theory predictions [10] (with the PDF set corresponding to the best fit and all scales chosen as $\mu_{R,F,f} = p_T^\gamma$) to the predictions with $\mu_{R,F,f} = 0.5p_T^\gamma$ and $2p_T^\gamma$ are shown on the plot by dotted blue curves. The uncertainties of the theoretical prediction caused by the CTEQ6.1M PDF uncertainties have been

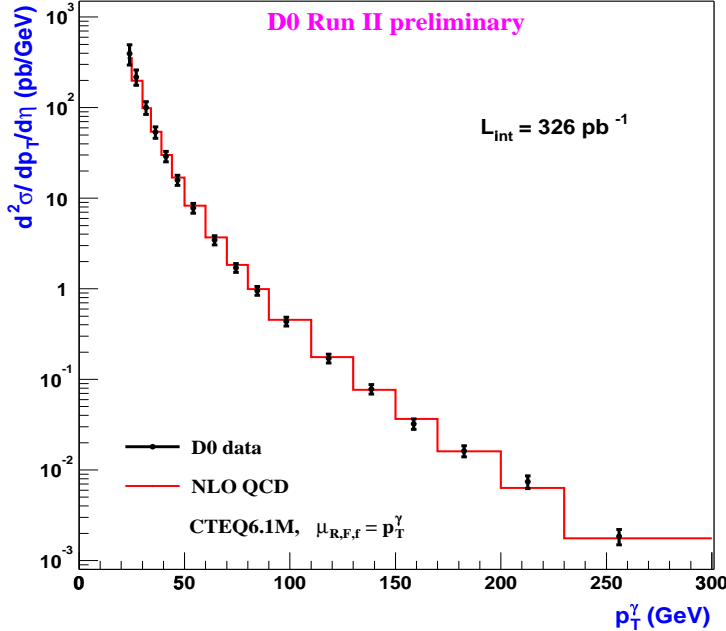


FIG. 4: The inclusive cross section for production of isolated photons $d^2\sigma/dp_T^\gamma d\eta$ vs. p_T^γ for the central ($|\eta| < 0.9$) pseudorapidity region. Total (systematic \oplus statistical) errors are shown. The histogram (red full line) is theoretical NLO QCD predictions [10] done for $\mu_R = \mu_F = \mu_f = p_T^\gamma$ with the CTEQ6.1M PDF set.

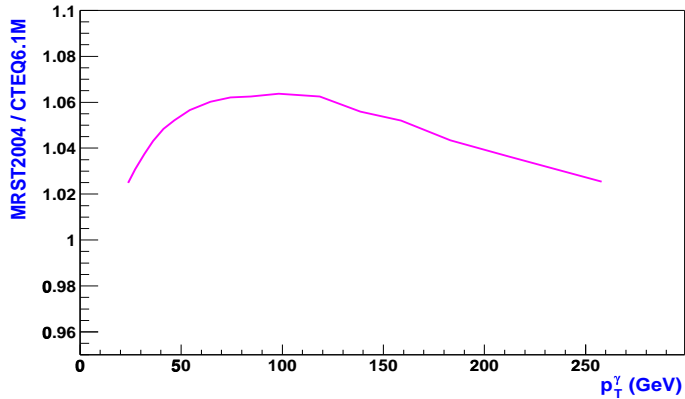


FIG. 5: Ratio of theoretical predictions with MRST2004 to those with CTEQ6.1M (statistical errors are less than 1%).

found using the 40 PDF sets [11]. These uncertainties are shown in Fig. 6 by the dash-and-dot red curves. They grow from 4-5% at $p_T^\gamma \simeq 25$ GeV to 9% at $p_T^\gamma \simeq 250$ GeV (with a tendency to grow at higher p_T^γ). A similar treatment using the approach of [12] yields comparable results, specifically a 1-2% variation, with similar p_T^γ dependence.

The NLO QCD predictions, both with CTEQ6.1M and MRST2004, describe the data within the experimental uncertainties in the whole p_T^γ range considered, $23 < p_T^\gamma < 300$ GeV. The presented measurements can be used in future PDF global fits (as it was done earlier, for example, in [17]), especially in the region of medium and high p_T^γ , where the experimental uncertainties from the inclusive jet cross sections are considerable. For this reason, extending the photon cross section to the region of larger p_T^γ would be very important.

Acknowledgments

We thank the staffs at Fermilab and collaborating institutions, and acknowledge support from the Department of Energy and National Science Foundation (USA), Commissariat à l'Energie Atomique and CNRS/Institut National de Physique Nucléaire et de Physique des Particules (France), Ministry of Education and Science, Agency for Atomic

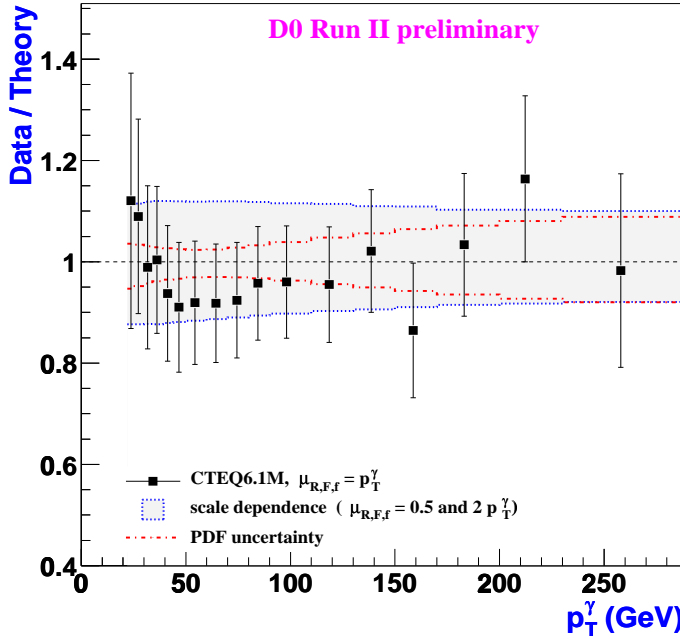


FIG. 6: The ratio of the measured cross section to the NLO QCD predictions done with [10] (theor. predictions based on the code [12] are within 7%), with the CTEQ6.1M PDF set is presented. Ratios of the nominal theory predictions (with $\mu_{R,F,f} = p_T^\gamma$ and CTEQ6.1M PDF set corresponding to the best fit) to the predictions with $\mu_{R,F,f} = 0.5p_T^\gamma$ (upper dotted blue curve) and $2p_T^\gamma$ (lower curve) as well as to the predictions with the largest upper and lower CTEQ6.1M PDF errors (dash-and-dot red curves) are also shown.

Energy and RF President Grants Program (Russia), CAPES, CNPq, FAPERJ, FAPESP and FUNDUNESP (Brazil), Departments of Atomic Energy and Science and Technology (India), Colciencias (Colombia), CONACyT (Mexico), KRF (Korea), CONICET and UBACyT (Argentina), The Foundation for Fundamental Research on Matter (The Netherlands), PPARC (United Kingdom), Ministry of Education (Czech Republic), Natural Sciences and Engineering Research Council and WestGrid Project (Canada), BMBF (Germany), A.P. Sloan Foundation, Civilian Research and Development Foundation, Research Corporation, Texas Advanced Research Program, and the Alexander von Humboldt Foundation.

- [1] E.L. Berger and J. Qiu, Phys.Rev. **D44** (1991)2002.
- [2] This measurement is described in detail in D0 Note 4672.
- [3] CDF Collaboration, F. Abe *et al.*, Phys.Rev. **D48** (1993)2998; F. Abe *et al.*, Phys.Rev.Lett. **73** (1994)2662;
- [4] DØ Collaboration, F. Abachi *et al.*, Phys.Rev.Lett. **77** (1996)5011; B. Abbott *et al.*, Phys.Rev.Lett. **84**(2000)2786; V. Abazov *et al.*, Phys.Rev.Lett. **87**(2001)251805.
- [5] DØ Collaboration, S. Abachi *et al.*, Nucl.Instrum.Methods **A338** (1994)185.
- [6] Proc. of CERN School of Computing, 1991, Ystad, Sweden, CERN 92-02, p.113 – 170.
- [7] C. Peterson, T. Rognvaldsson and L. Lonnblad, Comput.Phys.Commun.**81** (1994)185 (version 3.5 is used here).
- [8] T. Sjostrand, Comp.Phys.Comm. **82** (1995)74.
- [9] R. Barlow, C. Beeston, Comp.Phys.Comm. **77** (1993)219-228.
- [10] P. Aurenche *et al.*, JETPHOX package, http://wwwlapp.in2p3.fr/lapth/PHOX_FAMILY/main.html.
S. Catani, M. Fontannaz, J.Ph. Guillet and E. Pilon, Preprint LAPTH-907/02, JHEP 0205 (2002)028, hep-ph/0204023.
- [11] J. Pumplin *et al.*, JHEP 0207 (2002)12; D. Stump *et al.*, JHEP 0310 (2003)046.
- [12] L.E. Gordon and W. Vogelsang, Phys.Rev. **D48** (1993)3136; L.E. Gordon and W. Vogelsang, Phys.Rev. **D50** (1994)1901.
- [13] L. Bourhis, M. Fontannaz, J.P. Guillet, Eur.Phys.J. **C2** (1998)529, hep-ph/9704447.
- [14] M. Gluck, E. Reya and A. Vogt, Phys.Rev. **D48**, (1993)116, [Erratum-ibid. D **51** (1995)1427].
- [15] These tests were done by W. Vogelsang with his QCD NLO code [12].
- [16] A.D. Martin *et al.*, Phys.Lett. **B604** (2004)61.
- [17] A.D. Martin *et al.*, Eur.Phys.J. **C4** (1998)463; W. Vogelsang and A. Vogt, Nucl.Phys. **B453** (1995)334; P. Aurenche *et al.*, Phys.Rev. **D39** (1989)39.